MATERIALS SCIENCE

Electrochemically mediated gating membrane with dynamically controllable gas transport

Yayuan Liu, Chun-Man Chow, Katherine R. Phillips, Miao Wang, Sahag Voskian, T. Alan Hatton*

The regulation of mass transfer across membranes is central to a wide spectrum of applications. Despite numerous examples of stimuli-responsive membranes for liquid-phase species, this goal remains elusive for gaseous molecules. We describe a previously unexplored gas gating mechanism driven by reversible electrochemical metal deposition/dissolution on a conductive membrane, which can continuously modulate the interfacial gas permeability over two orders of magnitude with high efficiency and short response time. The gating mechanism involves neither moving parts nor dead volume and can therefore enable various engineering processes. An electrochemically mediated carbon dioxide concentrator demonstrates proof of concept by integrating the gating membranes with redox-active sorbents, where gating effectively prevented the cross-talk between feed and product gas streams for high-efficiency, directional carbon dioxide pumping. We anticipate our concept of dynamically regulating transport at gas-liquid interfaces to broadly inspire systems in fields of gas separation, miniaturized devices, multiphase reactors, and beyond.

INTRODUCTION

The design of stimuli-responsive membranes capable of regulating substance transport at the nanoscale is a subject of intense research, motivated by the broad potential impact on science and technology (*1*–*5*). To date, a wide variety of functional membranes have been investigated with tunable permeability/selectivity of species in the liquid phase (solvents, ions, and dissolved organic molecules) (*1*–*3*). However, the control of gas molecule transport at gas-liquid interfaces remains largely unexplored (*6*, *7*), mainly due to the smaller sizes and greater diffusivities of both free and dissolved gas molecules, as well as the spontaneous interfacial mass transfer necessary to establish vapor-liquid equilibrium (*8*, *9*). Nevertheless, the ability to modulate transport behavior dynamically at a gas-liquid interface is crucial to a wide spectrum of emerging energy, biomedical, and chemical engineering applications, including fluidic control in miniaturized devices (*10*), gas-involved chemical reactions (*11*, *12*), controlled gas exchange (*13*), and directional gas pumping (*14*).

Nearly all the reported micro/nanoscale gas gating mechanisms are confined to the field of microelectromechanical systems (MEMS), which usually involve mechanical moving parts coupled to magnetic, electric, pneumatic, or thermal actuation methods (*10*). However, such designs often inevitably introduce dead volume to the system and are challenging to realize low leakage rates, which can severely compromise the effectiveness of gas gating (*15*). Moreover, MEMS-based gas valves may also suffer from laborious and expensive fabrication, mechanical instability, and high energy consumption, hindering their compatibility with large-scale applications. On the other hand, membrane-based systems for controllable gas transport have only been demonstrated very recently using liquid-infused microporous membranes, where gases can only permeate through the membrane on deformation of the pore-filling gating liquid meniscus above a specific pressure threshold (*6*, *7*, *16*–*20*). Despite being a major breakthrough, the realization of continuous permeability adjustment in liquid-infused membranes may not be straightforward (*7*). Therefore, the development of smart gating membranes with dynamic and reversible control over gas transport behavior is still in its infancy, making research effort in this direction critically needed.

Here, we propose a new strategy to continuously and dynamically modulate gas transfer at a gas-liquid interface, based on reversible electrochemical metal deposition/dissolution (zinc, Zn) on conductive porous membranes at the gas-liquid interface. The high-porosity, low-tortuosity membrane ensured rapid gas transport at the gas-electrolyte interface in the open state (Fig. 1A). Through detailed study on the relationship between electrolyte formulation and the electrochemical nucleation behavior, highly reversible cycling of metallic Zn [>99% Coulombic efficiency (CE)] can be realized with excellent kinetics and deposition homogeneity. As a result, a compact and uniform layer of Zn nanocrystals can be formed on the membrane with minimum deposition capacity, affording an effective gas barrier within at most a few minutes (Fig. 1B). By adjusting the amount of electrodeposited metal, a continuous-state tuning of gas permeability can be achieved for the first time, with values spanning over two orders of magnitude. The reported gating mechanism requires much lower power input compared to conventional designs for fluid control and does not require continuous energy input to maintain the operational state. Moreover, this electrochemically mediated gas gating approach neither involves mechanical moving parts nor introduces dead volume between switching. Such configurational advantages are particularly desirable in processes such as membrane-based gas separation, which can offer higher efficiency, easier operation, and a smaller footprint compared to conventional batch processes (*21*).

To highlight the versatility of our gating approach, an electrochemical carbon dioxide (CO_2) separation device is demonstrated by sandwiching a redox-active CO_2 sorbent electrode between two gating membranes (Fig. 1, C and D), with the two electrochemical circuits (gating and CO_2 capture/release) sharing the same electrolyte. In this novel setup, Zn shuttling between the gating membranes can open one gate while simultaneously closing the other, and quinone-based CO_2 carriers, which are immobilized on a conductive porous substrate, can reversibly bind/release CO_2 in their reduced/oxidized form, respectively (*14*, *22*–*24*). During capture, the

Department of Chemical Engineering, Massachusetts Institute of Technology, Cambridge, MA 02139, USA.
*Corresponding author. Email: tahatton@mit.edu

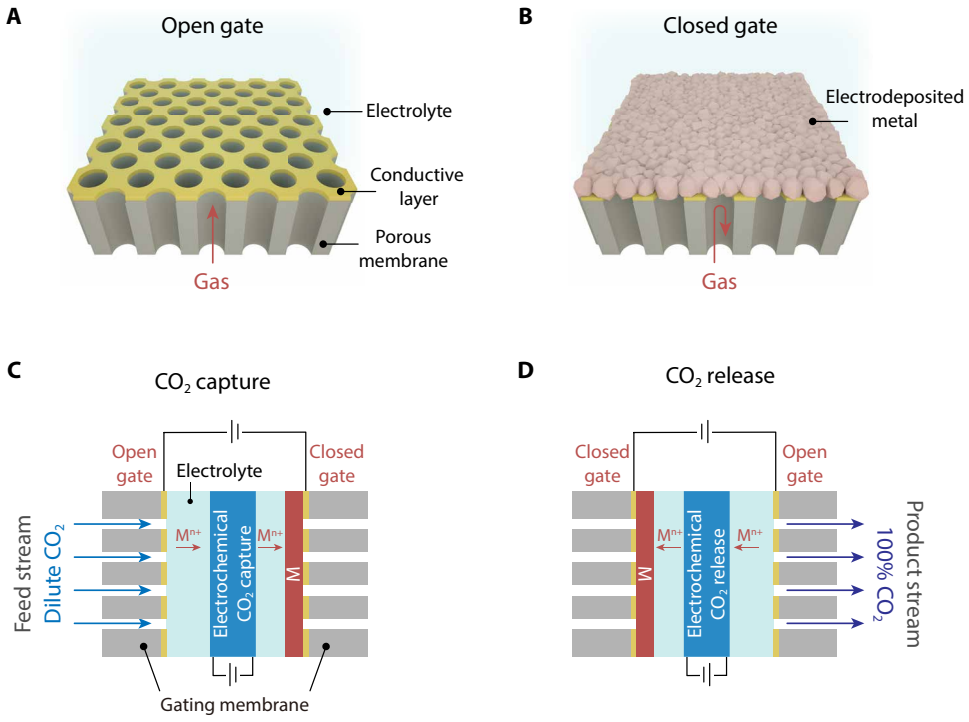

Fig. 1. Schematics showing the working principles of an electrochemically mediated gas gating membrane. (**A**) Gating membrane in its open state, where the AAO membrane with ordered one-directional pores allows rapid mass transfer to the gas-liquid interface. The top surface of the membrane is rendered electrically conductive via physical deposition of a gold thin film. (**B**) Gating membrane in its closed state. Electrodeposition of a dense metallic nanocrystal layer on the conductive membrane surface can afford an effective gas barrier to reduce the membrane permeability. (**C** and **D**) Operational modes of the electrochemically mediated CO_2 concentrator demonstrated in this work, which is constructed by integrating an electrochemical CO_2 capture cell with two gating membranes. Quinone molecules serve as the redox-active sorbents for CO_2 capture/release, which can form stable CO_2 adducts when being reduced and release CO_2 when being oxidized. M denotes an electrochemically deposited metal coating, which is Zn in this study. M^{n+} denotes the corresponding cation of M, which is Zn^{2+} in this study. (C) For CO_2 capture, the gate is open toward a dilute feed stream, and the quinone electrode is being reduced to absorb CO_2. (D) For CO_2 release, the gate polarity switches to open toward the product stream, and the quinone electrode is electrochemically oxidized to release pure CO_2.

system opens toward a dilute feed stream to continuously absorb CO_2 by the reduced sorbent, with the product-side gate closed (Fig. 1C). Once the sorbent capacity is reached, the feed-side gate is closed and the product-side gate is open, liberating pure CO_2 into the product stream via electrochemical sorbent oxidization (Fig. 1D). Because of the gating mechanism, the system can only access one gas stream at a time during operation, which greatly improves the separation efficiency by minimizing cross-talk between feed and product. As a result, our device can directionally pump low-concentration CO_2 against a chemical potential gradient to near purity using electricity as the sole driving force, with no upstream compressor or downstream vacuum needed. The transport behavior of this CO_2 separation system is further modeled with COMSOL Multiphysics, where good agreement with experimental data can be found. Integrating units operating at opposite polarity will allow an effectively continuous CO_2 capture-release process with compact footprint, and the demonstrated concept can also be extended to other separation scenarios, breaking ground for niche gas separation applications (*25*–*29*).

RESULTS AND DISCUSSION

Design rationale for the electrochemically mediated gas gating membrane

Vacuum-deposited metal thin films have been known to impart outstanding gas barrier properties to polymeric substrates and are extensively used today in applications ranging from food packaging to microelectronics (*30*). Therefore, the concept of dynamically modulating membrane gas permeability via reversible metal deposition/dissolution is highly feasible, provided important design criteria need to be fulfilled.

First, a high-porosity membrane is desirable for rapid gas transport in the open state, while the pore size should be small to minimize the amount of metal plating needed to achieve full pore blockage. Such material requirements make anodic aluminum oxide (AAO) an ideal candidate, as it exhibits well-defined one-directional channels with high pore density and a narrow pore size distribution (~100 nm in our case; Fig. 2, A and C). Other membranes such as porous battery separators and track-etched membranes can also be considered. A gold (Au) thin film (100 nm) was thermally evaporated for gating metal deposition on one side of the AAO to render it electrically conductive (Fig. 2, B and D, and fig. S1).

Second, the gating metallic species needs to have satisfactory deposition/dissolution kinetics for fast gating response. Redox couples such as Li^+/Li^0, Na^+/Na^0, Mg^{2+}/Mg^0, and Zn^{2+}/Zn^0 generally fall into this category and are therefore being actively pursued as anodes for rechargeable batteries (*31*). However, metallic Li, Na, and Mg are plagued with high (electro)chemical reactivity due to their low redox potentials (fig. S2), making them incompatible to interface with gaseous environments (*31*, *32*). Zn is uniquely positioned for gas gating applications with advantageous features of good air stability, low cost, and environmental benignity (*33*).

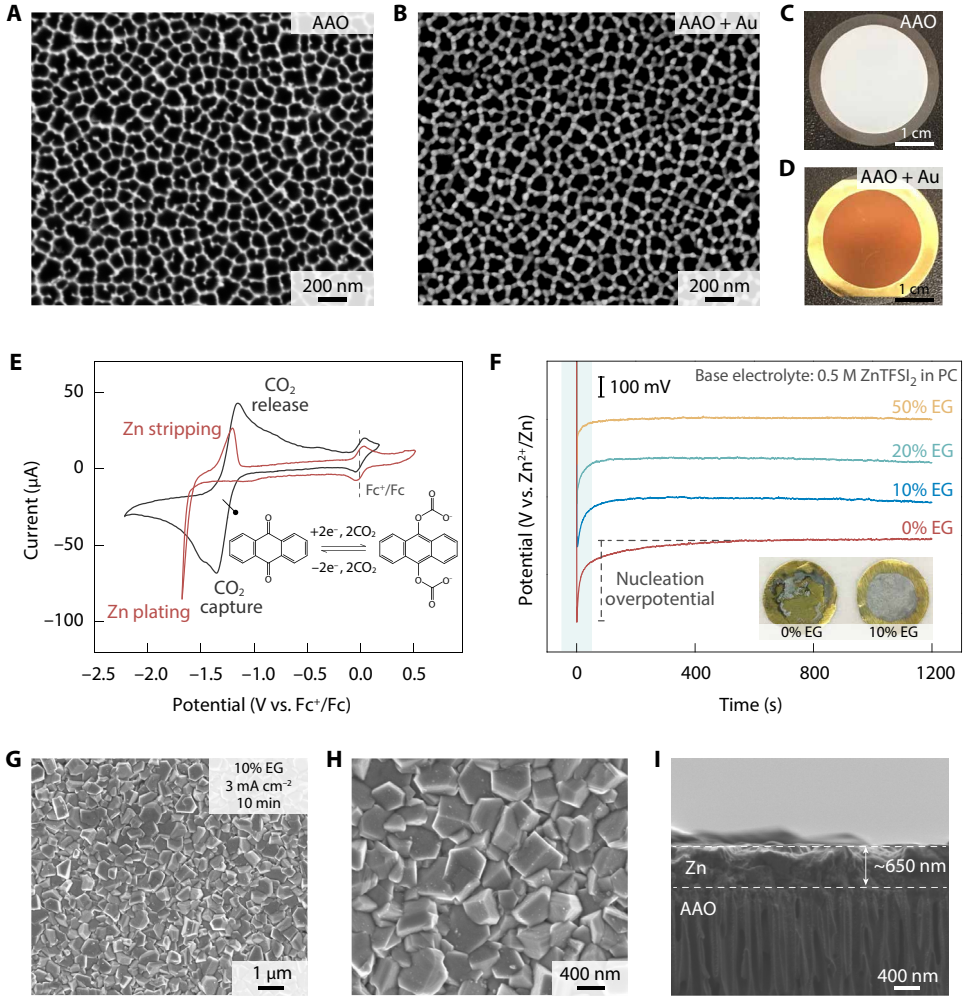

Fig. 2. Design rationale for the electrochemically mediated gas gating membrane. SEM images of (**A**) pristine and (**B**) Au-coated AAO membrane. Photo images of (**C**) pristine and (**D**) Au-coated AAO membrane. The AAO is peripherally bonded to an annular polypropylene supporting ring for ease of handling. Photo credit: Yayuan Liu, Massachusetts Institute of Technology. (**E**) CV of 1.0 M $Zn(NO_3)_2$ in dimethyl sulfoxide (red curve) and 5 mM anthraquinone in dimethyl sulfoxide with 0.1 M tetrabutylammonium hexafluorophosphate supporting salt under CO_2 atmosphere (black curve). The scan rate was 50 mV/s. The inset shows the reversible reaction between anthraquinone and CO_2. (**F**) Voltage profiles of Zn deposition on Au-coated aluminum foil in 0.5 M $ZnTFSI_2$ PC electrolyte with different amounts of EG additive. The deposition was carried out at a current density of 0.5 mA cm^{-2}, and slurry-coated Zn powder was used as the counter electrode to minimize the polarization contribution from the counter electrode. For better visual comparison, the profiles are shifted vertically. The inset shows the photo image of deposition without EG and with 10% EG as additive. Photo credit: Yayuan Liu, Massachusetts Institute of Technology. (**G** and **H**) Top-view and (**I**) side-view SEM images of Zn deposition on AAO obtained in 0.5 M $ZnTFSI_2$ PC electrolyte with 10% EG. The deposition was carried out at a current density of 3 mA cm^{-2} for 10 min.

It is worth noting that if the gating membrane were to be coupled with another electrochemical process sharing the same electrolyte, then the redox potential of that process should be more positive than that of Zn^{2+}/Zn^0 to avoid interference by Zn^{2+} in the electrolyte. This is valid for the quinone-based CO_2 capture/release process demonstrated in this study, as can be seen from the cyclic voltammetry (CV) scans in Fig. 2E. The electrochemistry of the quinone electrode will be discussed in greater detail in a later section. The potential of Zn^{2+}/Zn^0 falls more negative than most of the practically relevant gas-involved electrochemical processes, such as electrochemically mediated gas capture (*23*, *24*, *34*) and organic electrosynthesis (*35*, *36*), rendering our gas gating membrane widely applicable.

Third, homogeneous electrodeposition with high reversibility is another prerequisite for effective gas gating. Aqueous Zn chemistry commonly used in battery research unfortunately suffers from low efficiency (<50% in typical alkaline solution) and dendritic deposition morphology (*33*). Therefore, a non-aqueous electrolyte needs to be used, which has rarely been studied in literature (*37*).

In this study, propylene carbonate (PC) was selected as the electrolyte solvent due to its wide electrochemical stability window and low volatility (*26*). We first studied the Zn plating morphology on Au-coated aluminum foil using 0.5 M zinc bis(trifluoromethanesulfonyl)imide ($ZnTFSI_2$) in PC. However, as seen from the scanning electron microscopy (SEM) images, Zn grew into large aggregates that only sparsely covered the substrate (fig. S3), which stands in stark contrast to the continuous thin film obtained in an aqueous electrolyte (fig. S4). This highly localized deposition behavior might be attributed to the relatively large interfacial energy between metallic Zn and PC. According to the classical nucleation theory, the Gibbs energy for nucleation is the sum of the bulk and the interfacial free

energy (*38*). High interfacial energy will therefore result in low nucleation density and aggregated deposition morphology to minimize the surface area. This hypothesis can be corroborated by the large nucleation overpotential observed for Zn deposition in PC, which is defined as the magnitude of the voltage spike at the onset of galvanostatic deposition (Fig. 2F). We found that ethylene glycol (EG) can be used as an electrolyte additive to effectively reduce the interfacial energy. The nucleation overpotential decreased continuously with increasing amount of EG, and the addition of merely 10 volume % EG can already afford a highly uniform Zn film (Fig. 2F, inset).

Figure 2 (G and H) shows the top-view SEM images of Zn deposits on an AAO membrane obtained in PC electrolyte with 10% EG additive at a high current density of 3 mA cm^{-2} for 10 min. A compact Zn film consisting of uniform, crystalline Zn polyhedrons can be observed, and the homogeneity persisted over the whole deposition area (fig. S5). A side-view SEM image indicates a tight coverage of the Zn film on the surface of AAO (Fig. 2I and fig. S6). The thickness of the film at a deposition capacity of 0.5 mAh cm^{-2} was ~650 nm, which agrees well with the theoretical value of a dense Zn layer (655 nm). The dense deposition morphology is highly desirable for effective gas gating. The Zn cycling CE, which is defined as the ratio between dissolution and deposition capacity, is also critical for reversible gas gating. Unprecedented CE can be achieved using our PC-based electrolyte, with a value of 99.3% at a high current of 3 mA cm^{-2} (fig. S7).

Ex situ testing of the electrochemically mediated gating membrane

One distinct advantage of the electrochemically mediated gating mechanism is its ability to modulate the membrane permeability continuously. This feature has been observed previously in membranes gated with redox-active polymers, which are particularly useful for flux control in the liquid phase (*39*, *40*). Here, a denser Zn film and more complete pore coverage can be observed with increasing deposition capacity, which, in turn, result in decreasing permeability (fig. S8). To verify the capability of continuous-state tuning, membranes with different amounts of Zn deposited were first evaluated ex situ in both the liquid and gas phase.

Liquid-phase diffusion experiments were conducted in an H cell configuration using methyl orange dye as a tracker. Methyl orange (1 mM) and pure water were separated by the membranes, and aliquots were taken from the permeate chamber to determine the crossover concentration via ultraviolet-visible (UV-vis) spectroscopy (fig. S9). As can be seen from Fig. 3A and fig. S10, the dye can diffuse rapidly through the membrane in its open state (pristine AAO), while the crossover rate decreased gradually with increasing Zn capacity until the color change was barely visible over 24 hours for the 0.5 mAh cm^{-2} Zn gated membrane. Quantitatively, the crossover concentration after 24 hours was 297 μM for pristine AAO, but was 28.7, 5.6, and 1.1 μM for 0.1, 0.3, and 0.5 mAh cm^{-2} Zn gated AAO, respectively (Fig. 3B). Thus, even a low deposition capacity of 0.1 mAh cm^{-2} (2-min deposition at 3 mA cm^{-2} current) can already slow down the dye diffusion by an order of magnitude, and 0.5 mAh cm^{-2} Zn effectively afforded a 300× reduction in membrane permeability.

Gas-phase gating, which is more demanding on the compactness of the gating metal layer, was also studied ex situ using CO_2 permeation as an example. In this experimental setup, 15% CO_2 (balance N_2) was passed via a mass flow controller (MFC) over one side of the membrane, and the permeated CO_2 was swept by pure N_2 toward an in-line gas analyzer to accurately determine the concentration (Fig. 3C). A detailed configuration of the gas cell is provided as fig. S11. As expected, the permeation flux for all membranes increased with increasing flow rate difference between the CO_2 feed and N_2 sweep streams, which corresponds to a higher transmembrane pressure (Fig. 3D and fig. S12). Consistent with liquid-phase experiments, the gas permeability of the membrane also decreased continuously with increasing Zn deposition under all flow conditions tested. Noticeably, no CO_2 permeation can be detected for 0.5 mAh cm^{-2} Zn gated AAO unless subjected to an extreme transmembrane pressure [200 standard cubic centimeters per minute (sccm) feed and 5 sccm sweep], which also translates into a two orders of magnitude reduction in gas permeability compared to the open-state membrane. The success of the above ex situ experiments in both the liquid and gas phase strongly demonstrates the effectiveness and wide tunability of our electrochemically mediated gating membrane.

In situ testing of the electrochemically mediated gas gating membrane

In situ testing of the electrochemically mediated gating membrane was conducted to further verify its ability to reversibly and dynamically control gas transport at the gas-liquid interface. The setup was similar to that used for ex situ testing, but the membrane was coupled with a mesh counter electrode with predeposited Zn (Fig. 4A and fig. S13). In the open state, CO_2 can transport through the electrolyte-imbibed separator via dissolution-diffusion and outgas into the sweep stream.

Figure 4B shows the sweep stream CO_2 concentration in response to gating (10-min deposition/dissolution at 3 mA cm^{-2}, with 10-min rest in between), where consistent gate on/off switching can be observed over 20 cycles. Looking at an individual cycle, the permeated CO_2 concentration kept decreasing with increasing Zn deposition until finally no crossover can be detected, followed by a gradual restoration of the open-state value with Zn dissolution (Fig. 4C). Note that the discrepancy between the onset of deposition/dissolution and the CO_2 signal response was due to system dispersion and the headspace volume of the flow chamber (fig. S14). Moreover, the in situ Zn cycling demonstrated an outstanding CE (averaged >99.5%; Fig. 4D) and stable voltage profiles (fig. S15), both providing strong evidence of the high reversibility of the gating membrane. The gating kinetics can be easily tuned by varying the cycling current while still maintaining a remarkable gating on/off ratio (Fig. 4E).

On the basis of the experimental data, the electrical energy required for complete on/off switching was calculated to be 518 mJ cm^{-2} (~0.144 mWh cm^{-2}) at a switching current of 3 mA cm^{-2}, which translates to an average power of 0.864 mW cm^{-2}. This energy/power input is orders of magnitude lower than those of conventional miniaturized valves involving mechanical actuation mechanisms (*10*). Moreover, unlike many other designs for fluid control, the electrochemically mediated gating membrane does not require continuous energy input to maintain its operational state, which further reduces the energy consumption.

High-efficiency electrochemical CO_2 separation enabled by gas gating membranes

To highlight the versatility of the gating approach, an electrochemical CO_2 concentrator is demonstrated here as a proof of concept, where the use of gas gating membranes enabled a new operating mode for gas separation by preventing the undesirable cross-talk

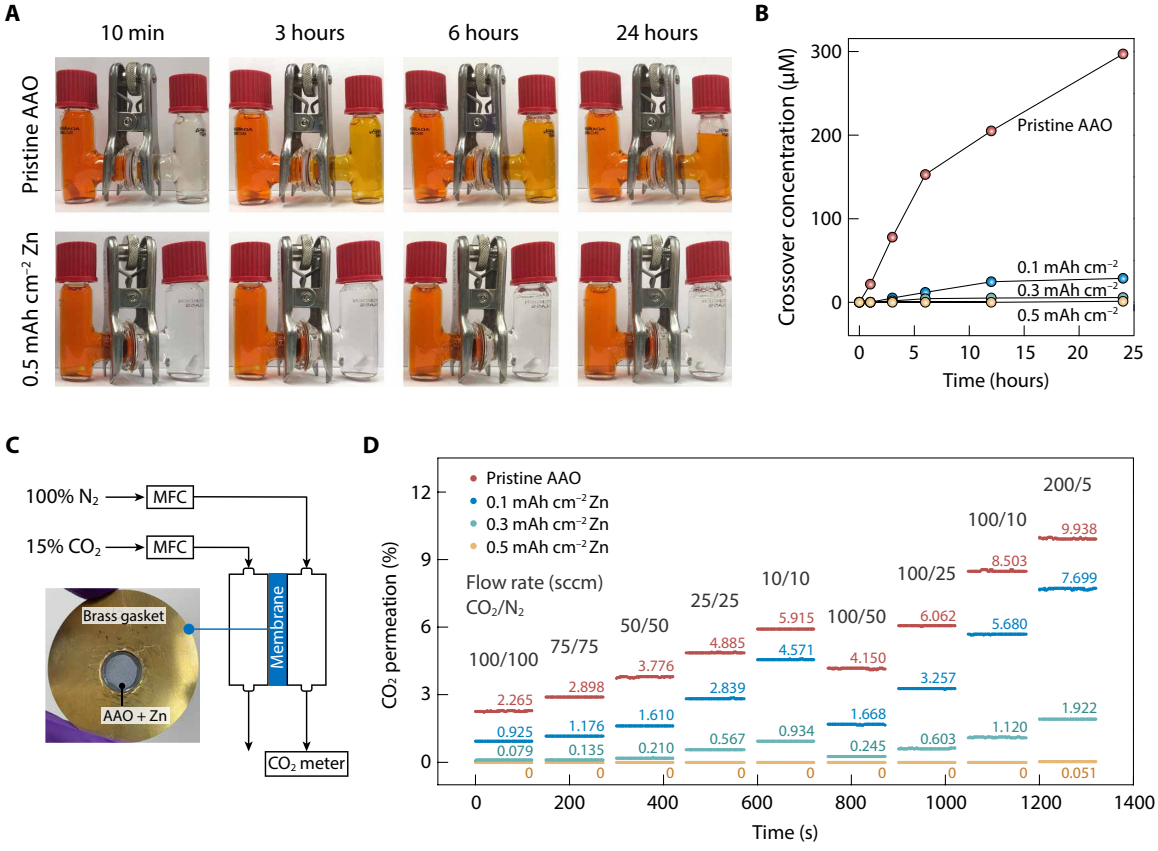

Fig. 3. Ex situ testing of the electrochemically mediated gating membrane. (**A**) Photo images showing the liquid-state diffusion tests at different time points for pristine AAO and 0.5 mAh cm^{-2} Zn gated AAO. Photo credit: Yayuan Liu, Massachusetts Institute of Technology. (**B**) Crossover dye concentration in the permeate chamber as a function of time for pristine AAO, and AAO gated with 0.1, 0.3, and 0.5 mAh cm^{-2} Zn. (**C**) Schematic illustrating the setup for ex situ gas-phase testing of the electrochemically mediated gating membrane. Membranes with different amounts of Zn deposited were mounted on brass gaskets, and the concentration of CO_2 permeated through the membranes was determined using an in-line CO_2 detector. Photo credit: Yayuan Liu, Massachusetts Institute of Technology. (**D**) CO_2 concentrations in the N_2 sweep stream under different gas flow conditions for pristine AAO, and AAO gated with 0.1, 0.3, and 0.5 mAh cm^{-2} Zn. The flow rates of the 15% CO_2 (balance N_2) feed stream and the N_2 sweep stream are indicated in the plot.

between the dilute and concentrated gas streams as well as obviating the need for system blowdown between absorption and desorption required in conventional temperature and pressure swing processes. It is worth emphasizing that various additional form factors are possible to incorporate the electrochemical gas gating membrane in gas separation (fig. S16), and our reported gas gating mechanism can also create opportunities in many other applications.

The development of high-efficiency CO_2 separation technologies is crucial for greenhouse gas mitigation, and of value in the petroleum, chemical, and heavy industries, as well as in specialty applications such as life support in confined spaces (*34*, *41*). One emerging strategy involves electrochemical cycles to capture/release CO_2, with quinones being a representative example (*14*, *22*–*24*, *26*). Electrochemically reduced quinones can bind to electrophilic CO_2 to form stable adducts, while the oxidation of the adducts regenerates the sorbents to release CO_2. A poly(1,4-anthraquinone) (PAQ)–carbon nanotube (CNT) composite was selected as the sorbent electrode (theoretical capacity, 260 mAh g^{-1} or 9.7 mmol CO_2 g^{-1}) (*42*). This material has recently been used by our group to demonstrate electro-swing–based CO_2 separation in a cyclic reactor configuration (*24*). To facilitate liquid-phase CO_2 mass transfer, PAQ was cast on a porous carbon felt 50 μm in thickness and paired with a $LiFePO_4$ (LFP) counter electrode (the PAQ-LFP electrode pair is termed the "CO_2 cell" hereafter). As seen from the capture-release voltage profiles, polarization increases with increasing PAQ mass loading and/or cycling rates, together with decreased capacity (Fig. 5A). Therefore, 0.75 mg cm^{-2} loading with 30-min capture/release (0.4 mA cm^{-2} current) was identified as an optimal cycling condition, under which satisfactory carbon capture capacity can be used while preserving good electrochemical kinetics and stability (Fig. 5B).

To prevent the system from operating beyond the mass transfer limit, the limiting current density of the CO_2 cell was estimated based on the diffusion model described in Fig. 5C (method S1). The limiting current is defined as the current when steady-state CO_2 concentration reaches zero at the depth of the PAQ electrode. CO_2 (15%) was used in the calculation, which is the approximate concentration expected in many carbon capture applications (*41*). The limiting current decreases with decreasing gas pressure and/or increasing electrode thickness, with the value being ~2 mA cm^{-2} for a 50-μm electrode under 1 atm pressure (Fig. 5D). Thus, the identified optimal PAQ cycling condition did not exceed the limiting current, yet was close enough to take sufficient advantage of kinetics. Operating slightly below the limiting current also allowed a smaller

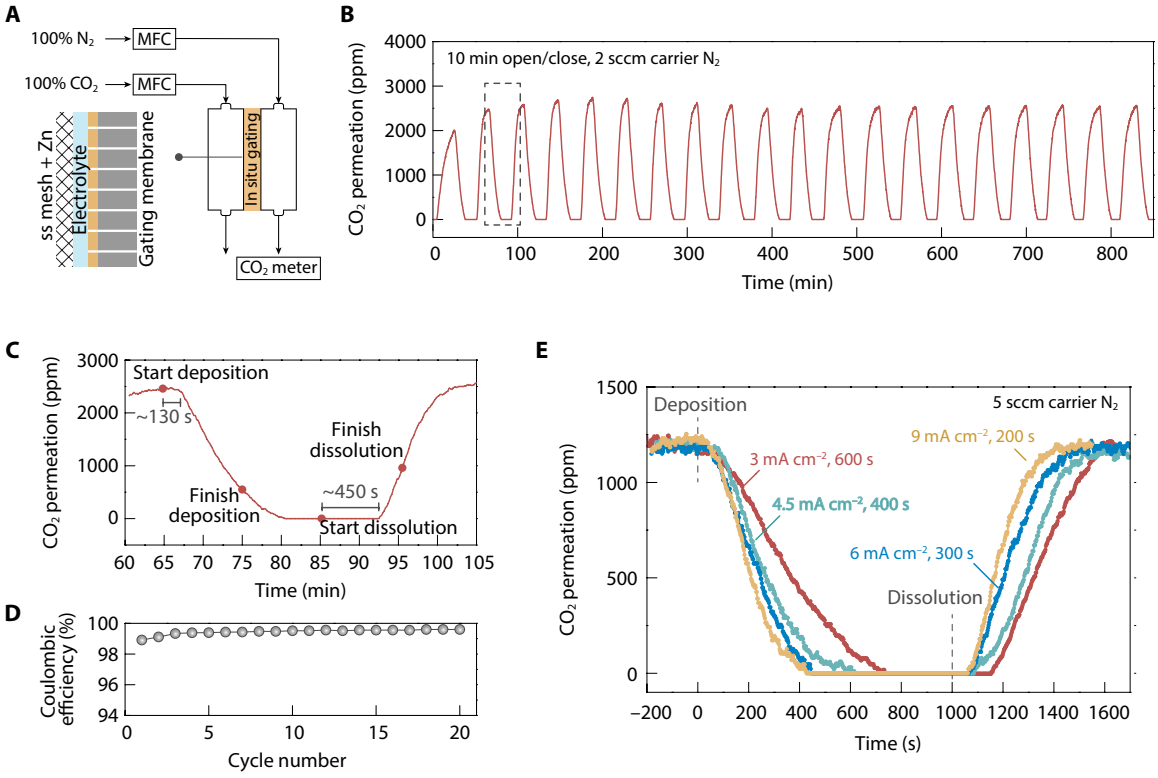

Fig. 4. In situ testing of the electrochemically mediated gas gating membrane. (**A**) Schematic illustrating the setup for in situ testing of the electrochemically mediated gas gating membrane. A stainless steel mesh with little impedance to gas flow was selected as the counter electrode. The testing used a "zero-gap" design, where both the membrane and the counter electrode were in close contact with the electrolyte-imbibed separator with no air gap in between, such that CO_2 crossover can only occur via dissolution-diffusion through the electrolyte. (**B**) Permeated CO_2 concentration in response to reversible gating (2 sccm N_2 as the carrier gas). The cycling protocol was 10-min deposition/dissolution at 3 mA cm^{-2}, with 10-min rest in between. (**C**) Detailed gating response of a single deposition/dissolution cycle marked with a dashed line in (B). The time lag between the onset of deposition/dissolution and the CO_2 signal response was due to system dispersion and the headspace volume of the testing device. (**D**) Zn cycling CE during in situ testing. (**E**) Gating responses under different Zn cycling current densities (5 sccm carrier gas). The deposition capacity was kept constant (0.5 mAh cm^{-2}).

gas-liquid contact area (size of the gating membrane) than the size of the CO_2 cell, which can reduce the gating energy consumption.

When the CO_2 cell was tested by flowing CO_2 on one side and N_2 on the other, a cyclic fluctuation of the permeated CO_2 concentration can be observed (Fig. 5E). During capture, CO_2 in the electrolyte was being actively consumed, resulting in a reduction in permeation, and a distinct concentration spike can be observed when PAQ was being oxidized to release the captured CO_2 (Fig. 5F). This behavior was verified through a COMSOL transport modeling, where the simulation predictions match closely with the experimental results (Fig. 5F). Details on the simulation can be found in method S2.

Nevertheless, a substantial CO_2 permeation background existed [~4500 parts per million (ppm) for the cycle shown in Fig. 5F] when the CO_2 cell was operated without a gating mechanism, due to the spontaneous CO_2 diffusion down the concentration gradient. In real gas separation scenario, if the CO_2 cell has access to both the dilute feed stream and the concentrated product stream, CO_2 will have a much higher tendency to be released back into the feed unless a sufficient differential pressure is created across the cell, which is detrimental to the separation efficiency (*14*, *21*). As a result, traditional gas separations using solid sorbents can only rely on batch processes, involving large-footprint columns, time- and energy-consuming system blowdown, and complex gas switching between different operating stages.

Integrating the CO_2 cell with our electrochemically mediated gas gating membranes offers an exciting opportunity to overcome the abovementioned barrier in separation efficiency. By sandwiching the CO_2 cell between two gating membranes in opposite on/off states (termed the "gating cell" hereafter), the system can only access one gas stream at a time to circumvent the undesirable cross-talk caused by chemical potential differences.

Figure 6A illustrates the configuration of the integrated CO_2 separation system, and detailed information is provided as fig. S17. The following design aspects were noted for high separation efficiency. (i) A "zero-gap" design was used, where the CO_2 cell and the gating cell were in tight contact without headspace or gas bubbles to avoid gas channeling (*43*). (ii) Minimum electrolyte was added such that the capture capacity of the CO_2 cell dominated over the physical CO_2 solubility in the electrolyte (method S3). (iii) The gating cell area (1 cm^2) was smaller than the CO_2 cell (6.45 cm^2) based on limiting current estimation to reduce gating energy consumption. (iv) The thickness of all components was reduced whenever possible to facilitate mass transfer. In real operation, the device would work by directionally pumping dilute CO_2 into a concentrated product. However, due to the limitation of our CO_2 detection method, an N_2 sweep was used in place of the product stream to monitor CO_2 capture/release with a gas sensor. The gating cell is defined as "closed"/"open"

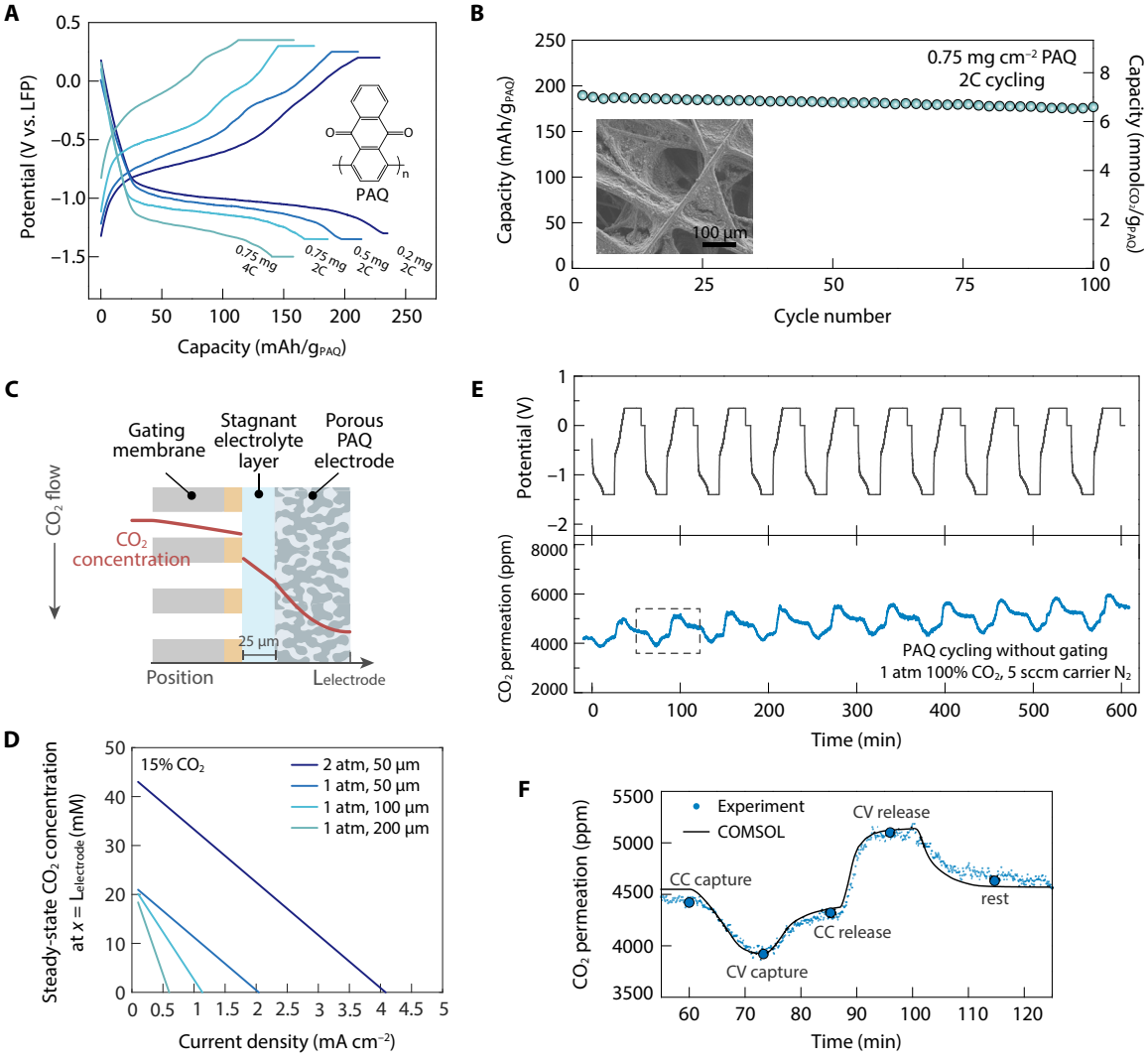

Fig. 5. Electrochemical properties of the redox-active quinone-based CO_2 sorbent. (**A**) CO_2 capture-release voltage profiles of PAQ electrodes with different mass loadings and cycling rates. 1C = 260 mA g^{-1} (capture/release in 60 min). The electrolyte was 0.1 M LiTFSI + 0.5 M $ZnTFSI_2$ in PC with 10% EG. (**B**) Cycling stability of PAQ with a mass loading of 0.75 mg cm^{-2} at 2C rate (0.4 mA cm^{-2}). The CO_2 capacity is calculated assuming 100% capture efficiency. Each capture/release step was 30 min following a constant current (CC)–constant voltage (CV) protocol. Inset shows the SEM image of the PAQ electrode. (**C**) Diffusion model for limiting current density calculation. (**D**) Steady-state CO_2 concentration at the depth of the PAQ electrode as a function of current density under different conditions. (**E**) CO_2 permeation in response to electrochemical cycling of the CO_2 cell, and the corresponding voltage profiles. Same device as gating membrane testing was used. (**F**) Detailed CO_2 permeation behavior during one capture-release cycle marked with a dashed line in (E), compared to the CO_2 permeation response predicted by COMSOL simulation. During CC capture, dissolved CO_2 was being consumed at a constant rate, resulting in a continuous decrease in permeation. When the cutoff voltage for CC capture was reached, CV capture started with decaying current density, resulting in a gradual restoration in CO_2 permeation. The subsequent CC release generated CO_2 at a constant rate, leading to a sharp concentration spike and the release rate decayed during CV release until permeation returned to its background value (~4500 ppm). The simulation predictions match closely with the experimental results.

when the system is accessing the feed/sweep stream, respectively (Fig. 6B). Thus, under this testing condition, metrics defining high-efficiency separation include no CO_2 crossover with the gate closed and a high concentration spike during CO_2 release with the gate open.

Figure 6C shows the typical behavior of the integrated separation system. Pure CO_2 was used as feed first to maximize the measurement sensitivity. No crossover can be detected when the gate was closed, confirming that the system was accessing only the feed stream during electrochemical CO_2 capture (red segment). After capture, we opened the gate by shuttling Zn to the other side of the gating cell, during which a gradual permeation increase appeared due to CO_2 outgassing from the electrolyte (teal segment). Subsequently, a distinct concentration spike was observed when the CO_2 cell was electrochemically oxidized to release CO_2 from the quinones (blue segment). Last, the CO_2 signal decayed back to zero on closing of the gate, thus completing a capture-release cycle (yellow segment). Consistent behavior was observed over multiple cycles (fig. S18). If we qualitatively compare the system efficiency by the ratio between the magnitude of the concentration spike and the permeation background, the value is ~0.39 for the integrated system, while it is only ~0.19 without the gating mechanism. Moreover, by lowering the feed concentration to more practical values (20% CO_2),

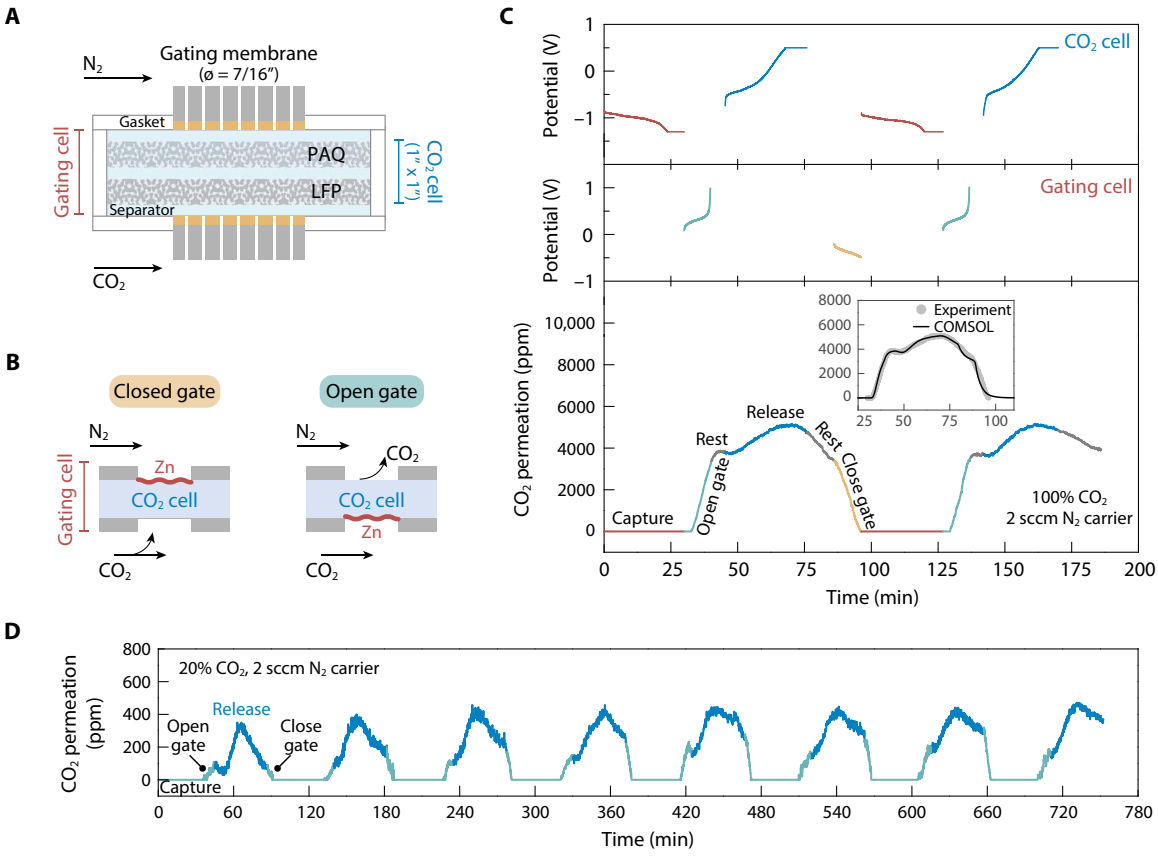

Fig. 6. High-efficiency CO_2 separation by integrating the CO_2 cell with two gas gating membranes. (**A**) Cross-sectional schematic of the integrated CO_2 separation system. Gating membranes were mounted on brass gaskets. PAQ and LFP electrodes were sandwiched between the gating membranes. The components were separated by electrolyte-imbibed polypropylene separators and confined with rubber gaskets without headspace. CO_2 flowed on one side of the device, and N_2 flowed on the other side to carry permeated CO_2 to the detector. (**B**) The gating cell is defined as closed when the system is facing the feed stream to capture CO_2, and as open when the system is facing the N_2 sweep stream to release CO_2. (**C**) CO_2 permeation during the operation of the integrated system, and the corresponding voltage profiles. The system started with a closed gate, and the CO_2 cell was electrochemically reduced to capture CO_2 (30-min CC-CV capture, red segment). Once the capture capacity was reached, the gating cell switched polarity and electrolyte outgassing caused CO_2 permeation to the sweep stream (Zn cycling at 3 mA cm^{-2} for 10 min, teal segment). The permeation increased first followed by a gradual decrease, because CO_2 in the electrolyte cannot be replenished from the feed side (gray segment). The captured CO_2 was then released from the CO_2 cell, resulting in a pronounced concentration spike (30-min CC-CV release, blue segment). The gate was finally closed by switching the gating cell polarity again to complete the cycle, with crossover concentration returned to zero (yellow segment). Inset shows the COMSOL simulation of the system response. (**D**) Continuous cycling of the integrated system with 20% CO_2 as the feed. Contribution from the CO_2 cell is marked in blue, and contribution from the physical solubility of the electrolyte is marked in teal.

transport to the product stream was dominated by the contribution from the CO_2 cell (Fig. 6D, contribution from the CO_2 cell is marked in blue and contribution from the physical solubility of the electrolyte is marked in teal). The results fulfilled our abovementioned metrics for high-efficiency separation. These phenomena were further validated using the corresponding COMSOL transport model simulation, where an excellent agreement with the experimental data was obtained (Fig. 6C, inset). The previous simulation model was adapted but with added gate closing/opening features, simulated as a temporal change in porosity that follows the gate closing/opening timing to reflect the zinc deposition/dissolution in the gating mechanism (method S2). The model allows the prediction of system performance at different gas compositions and operation parameters, paving the way for more comprehensive system-level modeling of such gas separation devices in the future.

The realization of reversible, dynamic transport control at a gas-liquid interface uniquely enabled directional CO_2 pumping without the need for differential pressure. Combining units operating at opposite polarities can afford an effectively continuous CO_2 capture-release process (fig. S19). Compared to conventional batch processes, our membrane-based "zero-gap" CO_2 separation device can obviate the need for system blowdown between absorption and regeneration, simplify reactor design, improve energy efficiency, and reduce the footprint of separation units for process intensification (*41*). Moreover, this novel gas separation process will also open unprecedented opportunities for niche applications, such as life support systems in manned space/marine missions and electrochemical gas compression (*28*, *29*).

Controlling transport behavior at gas-liquid interfaces is a largely under-researched topic, albeit being crucial for emerging technologies. In this work, we propose a novel gating mechanism capable of dynamically and continuously modulating gas transport at a gas-liquid interface, driven by electrochemical metal deposition/dissolution on conductive porous membranes in a rationally formulated electrolyte. The gas gating membrane can operate with low power consumption, and excellent on/off ratio, reversibility, kinetics, and tunability as verified by both ex situ and in situ testing. Moreover,

actuated only by electrochemistry, the gating membrane involves neither moving parts nor headspace, which is desirable for high gating efficiency and reliability. As a proof of concept, a compact, electrochemically mediated carbon dioxide separation device is achieved by sandwiching a redox-active CO_2 sorbent electrode between two gating membranes. The gating mechanism effectively minimized crosstalk between feed and product streams such that ideally the integrated device can directionally pump CO_2 against a concentration gradient without the need for differential pressure, making it versatile for diverse carbon capture applications. We anticipate that our concept of dynamically regulating mass transfer at gas-liquid interfaces will inspire applications in wide fields ranging from gas separations to miniaturized energy/medical devices to microscale gas-involved reactors and beyond.

MATERIALS AND METHODS

Materials

AAO membranes were purchased from Whatman (Anodisc 6809-6012, 25 mm diameter, 100 nm pore size) and rendered electrically conductive by depositing 100-nm Au on one side of the membrane via thermal evaporation. The electrolytes were prepared by dissolving the corresponding salts zinc bis(trifluoromethanesulfonyl)imide (Alfa Aesar), lithium bis(trifluoromethanesulfonyl)imide (Solvay), and/or tetrabutylammonium hexafluorophosphate (Sigma-Aldrich) in PC (anhydrous, 99.7%, Sigma-Aldrich), EG (anhydrous, 99.8%, Sigma-Aldrich), and/or dimethyl sulfoxide (Sigma-Aldrich). PC and EG were dried over molecular sieves (4 Å, Sigma-Aldrich) before use. Ferrocene and anthraquinone were purchased from Sigma-Aldrich.

Characterizations

SEM images and energy-dispersive x-ray elemental mappings were taken with a Zeiss SUPRA 55-VP scanning electron microscope. Liquid-phase diffusion tests were carried out in 5-ml H cells (Adams & Chittenden Scientific Glass). The two chambers were separated by an AAO membrane with a 0.5-cm^2 effective area. Methyl orange concentration in liquid-phase diffusion tests was determined using a UV-vis spectrometer (Ocean Optics). For CV measurements, glassy carbon (Ø 3 mm) was used as the working electrode, Pt wire was used as the counter electrode, Ag wire was used as a pseudo-reference electrode, and 1 mM ferrocene (Fc) was used as an internal reference.

Electrochemical Zn cycling

All the electrochemical measurements were conducted using a VersaSTAT4 potentiostat (Princeton Applied Research). To study the Zn deposition morphology, either Au-coated AAO or Au-coated aluminum foil was used as the substrate. The deposition was carried out in a pouch cell configuration with glass fiber separator (MilliporeSigma) and Zn foil (0.25 mm thick, Thermo Fisher Scientific) counter electrode. Zn foil was polished progressively down to 7000 grit sandpaper before use. For the study of nucleation overpotential, Zn dust (<10 μm, Sigma-Aldrich) counter electrode was used, which was fabricated by mixing 80% Zn dust, 10% carbon black (Super P, MTI Corp.), and 10% polyvinylidene fluoride (Sigma-Aldrich) in *N*-methylpyrrolidinone followed by slurry coating on aluminum foil.

Ex situ and in situ gas cell measurements

The gas-phase measurements were conducted using a house-machined device consisting of two gas flow chambers separated by the gating membrane, all held together with rubber gaskets and screws (detailed gas cell configuration shown as fig. S11). Membranes were mounted on brass holder discs using 5-min epoxy glue (Devcon). CO_2 of different concentrations flowed through one gas chamber, and N_2 sweep gas flowed through the other. The concentration of CO_2 in the N_2 stream was measured with an in-line CO_2 sensor (ExplorIR-W 20% CO_2 sensor). The sensor has a measurement range of 0 to 20% CO_2 and an accuracy of ±70 ppm. For in situ testing of the gas gating membrane, the membrane was coupled with a stainless steel mesh (316 stainless steel, 100 mesh, McMaster-Carr) counter electrode with predeposited Zn, and the two electrodes were separated by glass fiber separator.

Testing of the CO_2 cell

PAQ was synthesized following a previously reported procedure (*44*). To obtain the PAQ-CNT composite, PAQ was dissolved in chloroform (1 mg ml^{-1}) using a probe sonicator (Cole-Parmer Ultrasonic Processor, pulser mode: on 5 s–off 3 s, 60% amplitude). Subsequently, CNT was added into the solution (1 mg ml^{-1}) and the mixture was sonicated for another 20 min to afford a homogeneous dispersion. The PAQ-CNT ink was then drop-cast on 50-μm carbon felt (Fibre Glast Carbon Fiber Veil). The LFP counter electrode was prepared by mixing 95% LFP (MTI Corp.), 2.5% carbon black, and 2.5% polyvinylidene fluoride in *N*-methylpyrrolidinone followed by drop-casting on 50-μm carbon felt (mass loading, 8 mg cm^{-2}). The PAQ electrode and the LFP electrode were separated with a 25-μm polypropylene separator (Celgard 3501). The electrochemical cycling of the CO_2 cell was carried out using constant current followed by constant voltage until the current decays to 20% the value of the constant current cycling. The electrolyte used was 0.1 M LiTFSI + 0.5 M $ZnTFSI_2$ in PC with 10% EG additive.

Testing of the integrated CO_2 separation system

Zn was predeposited on one of the AAO membranes (0.6 mAh cm^{-2}, 0.5 mAh cm^{-2} Zn cycling capacity plus 20% extra to compensate Coulombic loss). The size of the PAQ electrode was 1 inch by 1 inch with an active material mass loading of 0.75 mg cm^{-2}. The size of the LFP electrode was 1″ by 1″ with an active material mass loading of 8 mg cm^{-2}. The AAO membranes and the electrodes were separated with 25-μm polypropylene separators and confined tightly using gaskets. CO_2 (100 or 20%) was used as the feed stream, and N_2 was used as a sweep stream for detection purpose. A complete capture and release cycle started with 30 min of CC-CV CO_2 capture with gate closed. Once the capture capacity was reached, the polarity of the gating cell was switched at 3 mA cm^{-2} for 10 min, followed by 5-min rest. Subsequently, CO_2 was released from the PAQ electrode by 30 min of CC-CV oxidation, followed by 10-min rest. Last, the cycle was completed by switching the polarity of the gating cell again (3 mA cm^{-2} for 10 min).

SUPPLEMENTARY MATERIALS

Supplementary material for this article is available at http://advances.sciencemag.org/cgi/content/full/6/42/eabc1741/DC1

REFERENCES AND NOTES

1. Z. Liu, W. Wang, R. Xie, X.-J. Ju, L.-Y. Chu, Stimuli-responsive smart gating membranes. *Chem. Soc. Rev.* **45**, 460–475 (2016).
2. Z. Zhu, D. Wang, Y. Tian, L. Jiang, Ion/molecule transportation in nanopores and nanochannels: From critical principles to diverse functions. *J. Am. Chem. Soc.* **141**, 8658–8669 (2019).

3. X. Hou, Smart gating multi-scale pore/channel-based membranes. *Adv. Mater.* **28**, 7049–7064 (2016).
4. S. Mura, J. Nicolas, P. Couvreur, Stimuli-responsive nanocarriers for drug delivery. *Nat. Mater.* **12**, 991–1003 (2013).
5. M. A. C. Stuart, W. T. S. Huck, J. Genzer, M. Müller, C. Ober, M. Stamm, G. B. Sukhorukov, I. Szleifer, V. V. Tsukruk, M. Urban, F. Winnik, S. Zauscher, I. Luzinov, S. Minko, Emerging applications of stimuli-responsive polymer materials. *Nat. Mater.* **9**, 101–113 (2010).
6. X. Hou, Y. Hu, A. Grinthal, M. Khan, J. Aizenberg, Liquid-based gating mechanism with tunable multiphase selectivity and antifouling behaviour. *Nature* **519**, 70–73 (2015).
7. Z. Sheng, H. Wang, Y. Tang, M. Wang, L. Huang, L. Min, H. Meng, S. Chen, L. Jiang, X. Hou, Liquid gating elastomeric porous system with dynamically controllable gas/liquid transport. *Sci. Adv.* **4**, eaao6724 (2018).
8. F. S. Gittleson, R. E. Jones, D. K. Ward, M. E. Foster, Oxygen solubility and transport in Li-air battery electrolytes: Establishing criteria and strategies for electrolyte design. *Energ. Environ. Sci.* **10**, 1167–1179 (2017).
9. P. V. Danckwerts, *Gas-Liquid Reactions* (McGraw-Hill Book Co., 1970).
10. K. W. Oh, C. H. Ahn, A review of microvalves. *J. Micromech. Microeng.* **16**, R13–R39 (2006).
11. M. Abolhasani, K. F. Jensen, Oscillatory multiphase flow strategy for chemistry and biology. *Lab Chip* **16**, 2775–2784 (2016).
12. R. Abdallah, V. Meille, J. Shaw, D. Wenn, C. de Bellefon, Gas-liquid and gas-liquid-solid catalysis in a mesh microreactor. *Chem. Commun.* **40**, 372–373 (2004).
13. M. Paven, P. Papadopoulos, S. Schöttler, X. Deng, V. Mailänder, D. Vollmer, H.-J. Butt, Super liquid-repellent gas membranes for carbon dioxide capture and heart-lung machines. *Nat. Commun.* **4**, 2512 (2013).
14. B. Gurkan, F. Simeon, T. A. Hatton, Quinone reduction in ionic liquids for electrochemical CO_2 separation. *ACS Sustain. Chem. Eng.* **3**, 1394–1405 (2015).
15. J. Goldowsky, H. F. Knapp, Gas penetration through pneumatically driven PDMS micro valves. *RSC Adv.* **3**, 17968–17976 (2013).
16. A. B. Tesler, Z. Sheng, W. Lv, Y. Fan, D. Fricke, K.-C. Park, J. Alvarenga, J. Aizenberg, X. Hou, Metallic liquid gating membranes. *ACS Nano* **14**, 2465–2474 (2020).
17. X. Hou, Liquid gating membrane. *Natl. Sci. Rev.* **7**, 9–11 (2020).
18. W. Liu, M. Wang, Z. Sheng, Y. Zhang, S. Wang, L. Qiao, Y. Hou, M. Zhang, X. Chen, X. Hou, Mobile liquid gating membrane system for smart piston and valve applications. *Ind. Eng. Chem. Res.* **58**, 11976–11984 (2019).
19. Y. Fan, Z. Sheng, J. Chen, H. Pan, B. Chen, F. Wu, S. Wang, X. Chen, X. Hou, Visual chemical detection mechanism by a liquid gating system with dipole-induced interfacial molecular reconfiguration. *Angew. Chem. Int. Ed.* **58**, 3967–3971 (2019).
20. H. Bazyar, S. Javadpour, R. G. H. Lammertink, On the gating mechanism of slippery liquid infused porous membranes. *Adv. Mater. Interfaces* **3**, 1600025 (2016).
21. J. R. Figueroa, H. E. Cuenca, in *Osmotically Driven Membrane Processes-Approach, Development and Current Status*, H. Du, A. Thompson, X. Wang, Eds. (IntechOpen, 2017), pp. 255–272.
22. M. B. Mizen, M. S. Wrighton, Reductive addition of CO_2 to 9,10-phenanthrenequinone. *J. Electrochem. Soc.* **136**, 941–946 (1989).
23. J. H. Rheinhardt, P. Singh, P. Tarakeshwar, D. A. Buttry, Electrochemical capture and release of carbon dioxide. *ACS Energy Lett.* **2**, 454–461 (2017).
24. S. Voskian, T. A. Hatton, Faradaic electro-swing reactive adsorption for CO_2 capture. *Energ. Environ. Sci.* **12**, 3530–3547 (2019).
25. M. P. Kang, J. Winnick, Concentration of carbon dioxide by a high-temperature electrochemical membrane cell. *J. Appl. Electrochem.* **15**, 431–439 (1985).
26. P. Scovazzo, J. Poshusta, D. DuBois, C. Koval, R. Noble, Electrochemical separation and concentration of <1% carbon dioxide from nitrogen. *J. Electrochem. Soc.* **150**, D91–D98 (2003).
27. H. Gao, L. Bai, J. Han, B. Yang, S. ZhanG, X. Zhang, Functionalized ionic liquid membranes for CO_2 separation. *Chem. Commun.* **54**, 12671–12685 (2018).
28. J. Knox, *Development of Carbon Dioxide Removal Systems for NASA's Deep Space Human Exploration Missions 2017–2018*, in 48th International Conference on Environmental Systems (2018).
29. Y. Tao, Y. Hwang, R. Radermacher, C. Wang, Experimental study on electrochemical compression of ammonia and carbon dioxide for vapor compression refrigeration system. *Int. J. Refrig.* **104**, 180–188 (2019).
30. M. A. Priolo, K. M. Holder, T. Guin, J. C. Grunlan, Recent advances in gas barrier thin films via layer-by-layer assembly of polymers and platelets. *Macromol. Rapid Commun.* **36**, 866–879 (2015).
31. H. Kim, G. Jeong, Y.-U. Kim, J.-H. Kim, C.-M. Park, H.-J. Sohn, Metallic anodes for next generation secondary batteries. *Chem. Soc. Rev.* **42**, 9011–9034 (2013).
32. D. Lin, Y. Liu, Y. Cui, Reviving the lithium metal anode for high-energy batteries. *Nat. Nanotechnol.* **12**, 194–206 (2017).
33. A. R. Mainar, E. Iruin, L. C. Colmenares, A. Kvasha, I. de Meatza, M. Bengoechea, O. Leonet, I. Boyano, Z. Zhang, J. A. Blazquez, An overview of progress in electrolytes for secondary zinc-air batteries and other storage systems based on zinc. *J. Energy Storage* **15**, 304–328 (2018).
34. M. C. Stern, F. Simeon, H. Herzog, T. A. Hatton, Post-combustion carbon dioxide capture using electrochemically mediated amine regeneration. *Energ. Environ. Sci.* **6**, 2505–2517 (2013).
35. M. Jouny, J.-J. Lv, T. Cheng, B. H. Ko, J. J. Zhu, W. A. Goddard, F. Jiao, Formation of carbon-nitrogen bonds in carbon monoxide electrolysis. *Nat. Chem.* **11**, 846–851 (2019).
36. S. Nitopi, E. Bertheussen, S. B. Scott, X. Liu, A. K. Engstfeld, S. Horch, B. Seger, I. E. L. Stephens, K. Chan, C. Hahn, J. K. Nørskov, T. F. Jaramillo, I. Chorkendorff, Progress and perspectives of electrochemical CO_2 reduction on copper in aqueous electrolyte. *Chem. Rev.* **119**, 7610–7672 (2019).
37. S.-D. Han, N. N. Rajput, X. Qu, B. Pan, M. He, M. S. Ferrandon, C. Liao, K. A. Persson, A. K. Burrell, Origin of electrochemical, structural, and transport properties in nonaqueous zinc electrolytes. *ACS Appl. Mater. Interfaces* **8**, 3021–3031 (2016).
38. A. Pei, G. Zheng, F. Shi, Y. Li, Y. Cui, Nanoscale nucleation and growth of electrodeposited lithium metal. *Nano Lett.* **17**, 1132–1139 (2017).
39. T. Hery, V.-B. Sundaresan, Ionic redox transistor from pore-spanning PPy(DBS) membranes. *Energ. Environ. Sci.* **9**, 2555–2562 (2016).
40. Y. Pan, S. Chou, H. K. Liu, S. X. Dou, Functional membrane separators for next-generation high-energy rechargeable batteries. *Natl. Sci. Rev.* **4**, 917–933 (2017).
41. M. C. Romano, R. Anantharaman, A. Arasto, D. C. Ozcan, H. Ahn, J. W. Dijkstra, M. Carbo, D. Boavida, Application of advanced technologies for CO_2 capture from industrial sources. *Energy Procedia* **37**, 7176–7185 (2013).
42. Z. Song, Y. Qian, M. L. Gordin, D. Tang, T. Xu, M. Otani, H. Zhan, H. Zhou, D. Wang, Polyanthraquinone as a reliable organic electrode for stable and fast lithium storage. *Angew. Chem. Int. Ed.* **54**, 13947–13951 (2015).
43. F. J. Navarro-Brull, R. Gómez, Modeling pore-scale two-phase flow: How to avoid gas-channeling phenomena in micropacked-bed reactors via catalyst wettability modification. *Ind. Eng. Chem. Res.* **57**, 84–92 (2018).
44. T. Yamamoto, H. Etori, Poly(anthraquinone)s having a .pi.-conjugation system along the main chain. Synthesis by organometallic polycondensation, redox behavior, and optical properties. *Macromolecules* **28**, 3371–3379 (1995).
45. D. T. Pritchard, J. A. Currie, Diffusion of coefficients of carbon dioxide, nitrous oxide, ethylene and ethane in air and their measurement. *J. Soil Sci.* **33**, 175–184 (1982).
46. P. D. Mantor, O. Abib Jr., K. Y. Song, R. Kobayashi, Solubility of carbon dioxide in propylene carbonate at elevated pressures and higher than ambient temperatures. *J. Chem. Eng. Data* **27**, 243–245 (1982).
47. R. Pohorecki, C. Możeński, A new absorbent for carbon dioxide and hydrogen sulphide absorption process. *Chem. Eng. Process* **37**, 69–78 (1998).
48. Y. Wang, C.-Y. Wang, K. S. Chen, Elucidating differences between carbon paper and carbon cloth in polymer electrolyte fuel cells. *Electrochim. Acta* **52**, 3965–3975 (2007).
49. T. C. Lourenço, S. Aparicio, G. C. Costa, L. T. Costa, Local environment structure and dynamics of CO2 in the 1-ethyl-3-methylimidazolium bis(trifluoromethanesulfonyl) imide and related ionic liquids. *J. Chem. Phys.* **146**, 104502 (2017).

Acknowledgments: We thank D. Calabro from the Corporate Strategic Research Laboratory of the ExxonMobil Research and Engineering Company for helpful discussions. **Funding:** The research was supported by ExxonMobil. **Author contributions:** Y.L. and T.A.H. conceived the concept and designed the experiments. Y.L. carried out the experiments with assistance from K.R.P. and M.W. C.-M.C. and Y.L. conducted simulations on the gating system. S.V. conducted quinone synthesis. T.A.H. supervised the project. Y.L. and T.A.H. prepared the manuscript with input from all the other coauthors. **Competing interests:** Y.L. and T.A.H. are inventors on a patent application related to this work filed by Massachusetts Institute of Technology (no. 63/002,490; filed on 31 March 2020). All other authors declare that they have no competing interests. **Data and materials availability:** All data needed to evaluate the conclusions in the paper are present in the paper and/or the Supplementary Materials. Additional data related to this paper may be requested from the authors.

Submitted 9 April 2020
Accepted 24 July 2020
Published 16 October 2020
10.1126/sciadv.abc1741

Citation: Y. Liu, C.-M. Chow, K. R. Phillips, M. Wang, S. Voskian, T. A. Hatton, Electrochemically mediated gating membrane with dynamically controllable gas transport. *Sci. Adv.* **6**, eabc1741 (2020).